

# Selectively-undercut traveling-wave electroabsorption modulators incorporating a p-InGaAs contact layer

Matthew M. Dummer, James R. Raring, Jonathan Klamkin, Anna Tauke-Pedretti, and Larry A. Coldren

University of California Santa Barbara, ECE Department, Santa Barbara, CA 93106 USA  
[dummer@engineering.ucsb.edu](mailto:dummer@engineering.ucsb.edu)

**Abstract:** A novel fabrication process has been developed for fabricating undercut-etched electroabsorption modulators that are compatible with tunable lasers. This process allows for the incorporation of highly doped p-type InGaAs above the upper cladding as an ohmic contact layer. The EAM demonstrates significant improvement in the microwave performance with little effect on modulation efficiency due to the undercut etching. This device uses a traveling wave electrode design with an integrated, matched termination resistor to demonstrate a 34 GHz 3-dB bandwidth for a 600  $\mu\text{m}$  long modulator.

© 2008 Optical Society of America

**OCIS codes:** (230.4110) Modulators; (230.4205) MQW modulators; (230.7020) Traveling-wave devices

---

## References and links

1. H. Kawanishi, H. Kawanishi, Y. Yamauchi, N. Mineo, Y. Shibuya, H. Mural, K. Yamada, and H. Wada, "EAM-integrated DFB laser modules with more than 40-ghz bandwidth," *IEEE Photon. Technol. Lett.* **13**, 954–956 (2001).
2. T. Knodl, C. Hanke, B. Saravanan, M. Peschke, R. Macaluso, and B. Stegmüller, "40 GHz monolithic integrated 1.3  $\mu\text{m}$  InGaAlAs-InP laser-modulator with double-stack MQW layer structure," in *Proceedings IEEE LEOS 17*, vol. 2, 2004, pp. 675–676 Vol.2.
3. J. Raring, L. Johansson, E. Skogen, M. Sysak, H. Poulsen, S. DenBaars, and L. Coldren, "40-Gb/s widely tunable low-drive-voltage electroabsorption-modulated transmitters," *J. Lightwave Technol.* **25**, 239–248 (2007).
4. H. Fukano, T. Yamanaka, M. Tamura, and Y. Kondo, "Very-low-driving-voltage electroabsorption modulators operating at 40 Gb/s," *J. Lightwave Technol.* **24**, 2219–2224 (2006).
5. T.-H. Wu, W.-C. Cheng, and D. Lee, "High-speed undercut-wet-etching-active-region traveling-wave electro-absorption modulator," in *Proceedings IEEE LEOS 18*, 2005, pp. 426–427.
6. Y.-J. Chiu, T.-H. Wu, W.-C. Cheng, F. Lin, and J. Bowers, "Enhanced performance in traveling-wave electro-absorption modulators based on undercut-etching the active-region," *IEEE Photon. Technol. Lett.* **17**, 2065–2067 (2005).
7. M. Sysak, J. Raring, J. Barton, M. Dummer, D. Blumenthal, and L. Coldren, "A single regrowth integration platform for photonic circuits incorporating tunable SGDBR lasers and quantum-well EAMs," *IEEE Photon. Technol. Lett.* **18**, 1630–1632 (2006).
8. D. Pasquariello, E. Bjorlin, D. Lasasoa, Y.-J. Chiu, J. Piprek, and J. Bowers, "Selective undercut etching of InGaAs and InGaAsP quantum wells for improved performance of long-wavelength optoelectronic devices," *J. Lightwave Technol.* **24**, 1470–1477 (2006).
9. R. Lewen, S. Irmscher, U. Westergren, L. Thylen, and U. Eriksson, "Segmented transmission-line electroabsorption modulators," *J. Lightwave Technol.* **22**, 172–179 (2004).
10. R. Spickermann and N. Dagli, "Experimental analysis of millimeter wave coplanar waveguide slow wave structures on GaAs," *IEEE Trans. Microwave Theory Tech.* **42**, 1918–1924 (1994).
11. L. A. Coldren and S. W. Corzine, *Diode Lasers and Photonic Integrated Circuits*, K. Chang, Ed. (John Wiley and Sons, Inc. 1995).

## 1. Introduction

Traveling-wave electroabsorption modulators (EAMs) in InP-based materials are attractive devices for optical fiber communications due to their compact size, high speed, and low drive voltage. These devices are also very well suited for monolithic integration with semiconductor lasers, allowing for minimal coupling loss and simple packaging of single-chip transmitters [1, 2, 3]. Recently, selective wet-etching of the waveguide core has been demonstrated to significantly increase the bandwidth of EAMs as well as to reduce the optical propagation loss. There have been several reports of such devices with bandwidths as high as 50 GHz in both InP/InAlGaAs [4] and InP/InGaAsP [5] [6] material systems. Typically, InP-based devices make use of lattice-matched indium gallium arsenide as an intermediate semiconductor layer, because the lower band-gap allows for good ohmic contacts. However, since InGaAs is susceptible to the same wet etch chemistries as InAlGaAs and InGaAsP, undercut EAMs have previously been limited to using highly doped p-InP instead as the upper metallization interface. This type of contact scheme is not ideal for integration with forward biased devices such as semiconductor lasers, because high-resistance contacts can lead to excess heat generation and lower optical output power.

In this work, we present the first undercut InGaAsP-region modulator which allows the incorporation of a p<sup>+</sup>-InGaAs contact layer. For these devices, we have developed a novel partial-sidewall mask process to protect the contact layer while leaving the waveguide core exposed to the selective wet etch. The material structure and fabrication process are compatible with those used for widely tunable sampled-grating (SG)DBR lasers. These EAMs show significantly improved performance due to the selective undercut as well as considerable bandwidth enhancement when operating in a traveling wave regime. We demonstrate EAMs up to 600  $\mu\text{m}$  long EAM with a 3-dB bandwidth in excess of 30 GHz and open eyes at 40 Gb/s. The dynamic extinction ratio for this device is 6.0 dB with a 1.6 V drive.

## 2. Material structure

Efficient EAMs have previously been integrated with SGDBR lasers using either a dual quantum well integration platform (DQW), where separate sets of QWs define the gain and modulation regions [7], or a quantum well intermixing platform (QWI), where the band edge of single set of QWs is shifted to achieve the desired functionality in each region [3]. The epitaxial layer structure for this device, grown by metal organic chemical vapor deposition (MOCVD), was designed to be compatible with either of these integration techniques (Fig 1(a)). The multi-quantum well (MQW) stack centered in the waveguide consists of ten 90  $\text{\AA}$  wells separated by nine 50  $\text{\AA}$  barriers with a band edge corresponding to a photoluminescence peak ( $\lambda_{PL}$ ) of 1465 nm. Although only a single growth is required for the EAM, the p-doped cladding was regrown separately to be consistent with laser fabrication.

## 3. Undercut fabrication

Fabricating the undercut waveguide requires deeply etching a ridge to expose the InGaAsP MQW material, followed by a selective wet-etch to reduce the core of the waveguide. We have chosen sulfuric acid, hydrogen peroxide, and DI water, mixed 1:1:10, as the undercut etchant, because of the high selectivity between InGaAsP and InP, and process repeatability. However, the lateral etch rate for InGaAs is more than 3 times faster than for InGaAsP [8], leading to the undesired removal of the contact layer during the undercut process. Fig. 1 shows a cross section

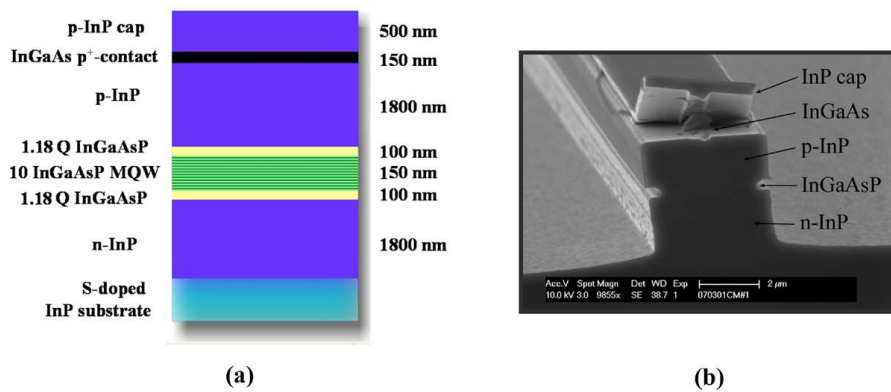


Fig. 1. (a) Epitaxial layer structure of undercut TW-EAM. (b) Cross section of ridge structure after 15 min. selective wet etch. The narrow InGaAs layer was broken during cleaving.

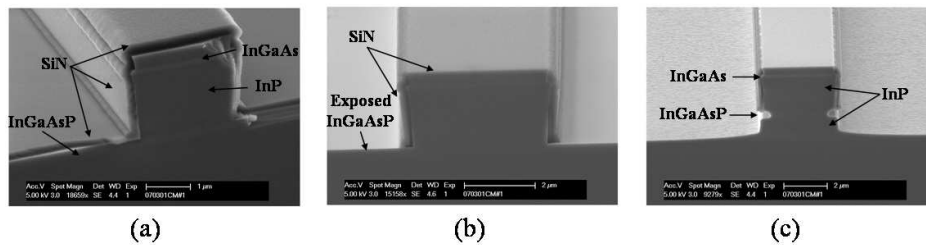


Fig. 2. Fabrication process for undercut EAM. (a) Surface ridge after 400 nm SiN deposition. (b) SiN nitride sidewall mask formation by vertical RIE. (c) Final cross-section after deeply etching ridge and 15 minute selective wet etching.

of a 3  $\mu\text{m}$  wide ridge after 15 minutes of selective wet etching. In this case, the InGaAsP was etched only 0.5  $\mu\text{m}$ , while the InGaAs layer was almost entirely removed.

During the modulator fabrication, it was therefore necessary to protect the InGaAs from the lateral etch before undercutting the waveguide core. This was accomplished by forming a partial sidewall mask, detailed in Fig. 2. First, the modulator ridge of the device was patterned using a 100 nm thick silicon nitride hard mask. The upper cladding was etched by methane-hydrogen-argon (MHA) reactive ion etching (RIE) followed by a hydrochloric/phosphoric acid (1:3) wet etch to stop exactly above the InGaAsP. A 400 nm-thick layer of SiN was then deposited by plasma enhanced chemical vapor deposition (PECVD). The SiN was subsequently etched by RIE using  $\text{CF}_4$ . Due to the anisotropy of the RIE, the SiN was preserved on the sidewalls of the ridges, while being completely removed from the horizontal surfaces. Active laser monitoring of the RIE prevented removal of the original 100 nm of SiN from the top of the ridge. This remaining SiN was then used as an in situ mask to deeply etch through the waveguide and lower cladding with MHA. Finally, a timed selective sulfuric-peroxide wet-etch was used to undercut the waveguide core. Figure 2(c) shows the final modulator geometry after etching for 15 minutes with the contact layer clearly intact.

Simulations of the optical mode profile have been performed to determine how the undercut etch effects the optical waveguide properties and modulation efficiency. Figure 3 shows the calculated overlap of the optical mode with the quantum wells as the core width is varied. For

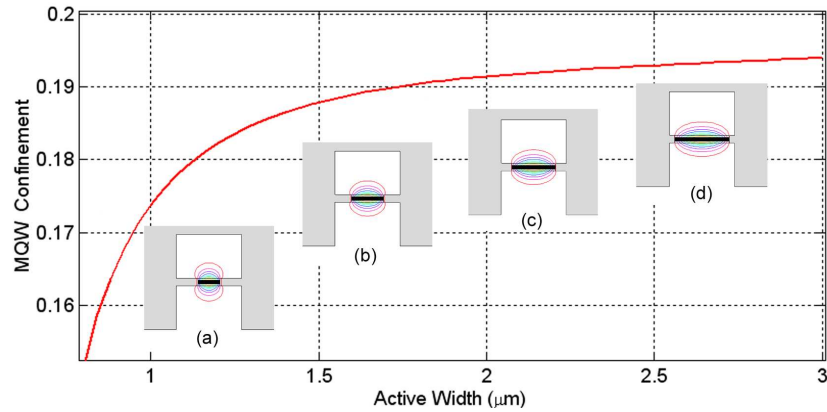


Fig. 3. Modal confinement in MQW active region vs quaternary waveguide width for 3  $\mu m$  wide cladding. Insets (a)-(d) depict mode profile for 1.0, 1.5, 2.0, and 2.5  $\mu m$  wide.

a waveguide core reduced from 3  $\mu m$  to 1.25  $\mu m$ , the difference in confinement is only 1% (0.194 to 0.184). However, for core widths less than 1  $\mu m$ , the modal overlap declines rapidly. This is evident from the mode profile contours which show more of the optical power leaking out into the cladding as the core becomes narrower.

#### 4. Modulator design

A photograph of the fabricated modulator is shown in Fig. 4(a). The device consisted of a surface ridge waveguide at the facets which tapered into undercut waveguide for the active modulator length. Using the fabrication technique described above, the core of the 3  $\mu m$  ridge was selectively wet-etched for 40 minutes to reduce the width to 1.4  $\mu m$ . A AuGe ground plane was defined on both sides of the ridge before the ridge was buried in benzocyclobutene (BCB) as a low-k dielectric. A via was etched through the BCB and the sacrificial InP cap layer was removed to expose the p-InGaAs prior to final Ti/Pt/Au metallization. The metal electrode was designed as a 600  $\mu m$  microstrip line such that the electrical and optical signals co-propagate along the length of the device. A coplanar waveguide (CPW) allowed for directly probing on one side of the transmission line while the opposite side was terminated with an integrated NiCr thin-film resistor. A metal-insulator-semiconductor (MIS) capacitor was also added to eliminate the DC power dissipation in the resistor [9]. A schematic depicting the completed device cross section is shown in Fig. 4(b).

#### 5. Electrical characterization

The TW-EAM has been characterized by electrical scattering parameter measurements. For these experiments, modulator test structures with CPW pads on both sides were fabricated to allow for 2-port electrical characterization with a vector network analyzer. We have compared the magnitudes of the  $S_{21}$  and  $S_{11}$  measurements for 600  $\mu m$  long EAMs with and without the selective undercut. The response of both devices is shown in Fig. 5 for -2.5 V DC bias. The undercut device clearly exhibits better microwave performance with greater bandwidth and much lower return loss. From the S-parameter data, the transmission line characteristics of the TW-EAM have been extracted using the ABCD matrix method [10]. As shown in Fig 6(a), the characteristic impedance is raised from 20  $\Omega$  to 28  $\Omega$  due to the capacitance reduction of the undercut etch.

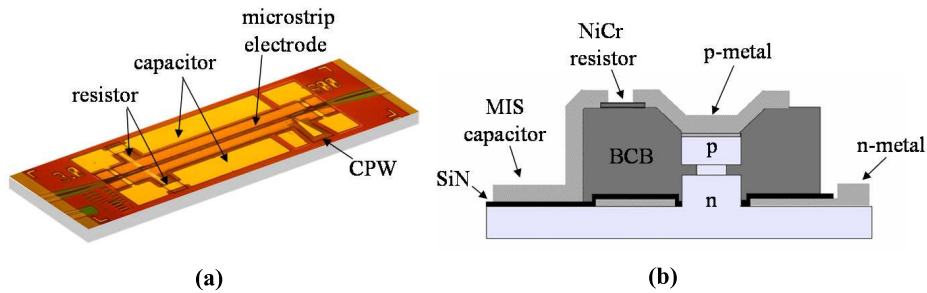


Fig. 4. (a) Fabricated TW-EAM with integrated resistor and capacitor termination. (b) Schematic cross-section of device and metallization layers.

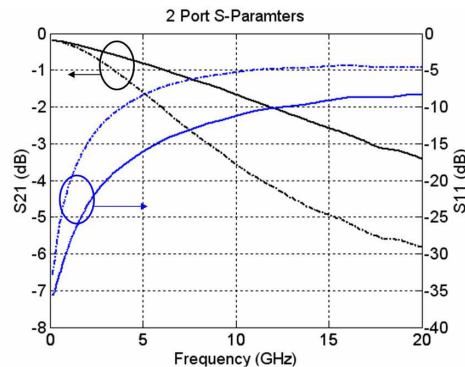


Fig. 5. Comparison of 2-port electrical S-parameters for TW-EAM with (solid) and without (dotted) undercut etching. DC bias is -2.5 V.

The electrical velocity in InP-based TW-EAMs is typically much lower than the optical velocity due to the slow-wave mode propagation induced by the diode capacitance. For long EAMs, this velocity mismatch can be a limiting factor for the bandwidth of the device. In InP/InGaAsP waveguides the optical group index is typically about 4 [11]. Fig 6 shows that with the undercut waveguide, the electrical index has been reduced from around 6 to 4, thereby achieving better velocity matching to the optical wave. The microwave loss has also been extracted for both devices as a function of frequency. Because the electrical attenuation coefficient ( $\alpha$ ) is dominated by the junction capacitance [12], the undercut is beneficial as well for improving the microwave loss.

## 6. Optical measurements

We have compared the modulation efficiency for the TW-EAM with and without the undercut etch. Figure 7(a) shows the DC extinction characteristics for both devices. For TE polarized light, the devices exhibit comparable extinction as predicted from the simulation, demonstrating that the undercut narrower waveguide does not effect the efficiency of the TW-EAM. Small signal electrical to optical (EO) responses have been measured for the undercut TW-EAM, shown in Fig. 7(b). A continuous wave optical signal was coupled through each facet to compare the forward and backward traveling-wave response. For a termination resistance of  $26 \Omega$ , the forward traveling 3-dB bandwidth is 34 GHz. In this case the device is well impedance matched and well velocity matched, so the bandwidth is limited almost entirely by the microwave loss. If

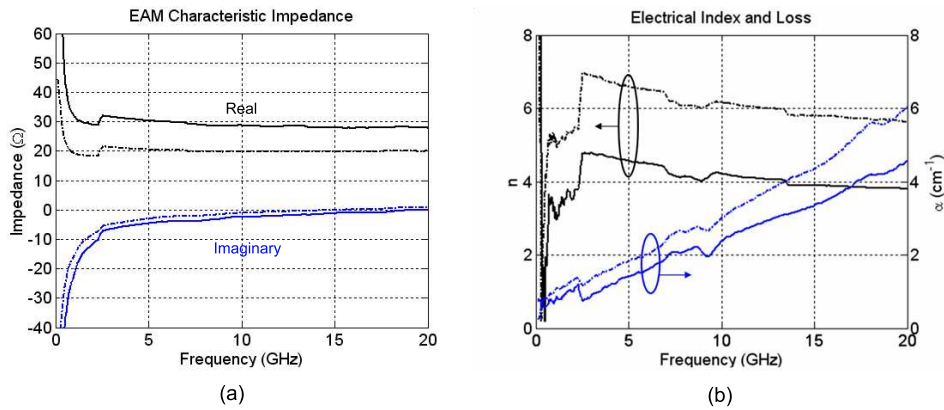


Fig. 6. (a) Characteristic impedance, and (b), microwave index and attenuation extracted from S-parameters. Solid lines and dotted lines denote devices with and without undercut etching, respectively.

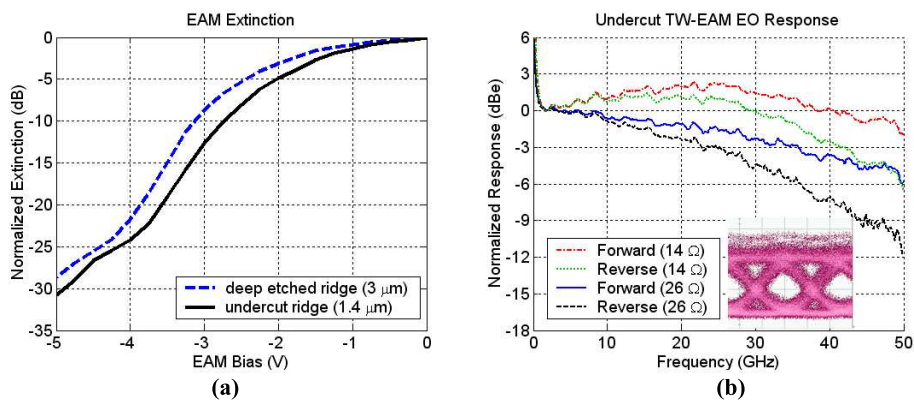


Fig. 7. (a) DC extinction characteristics of EAM with and without undercut for  $\lambda = 1550\text{nm}$ . (b) Traveling-wave frequency response for the  $600\ \mu\text{m}$  long undercut EAM. The inset shows the 40 Gb/s (PRBS  $2^{31} - 1$ ) eye for the forward traveling 26  $\Omega$  case.

the EAM is terminated with a resistance lower than the characteristic impedance, the reflected RF power adds constructively to the forward traveling power to generate an enhancement in the response. With a 14  $\Omega$  termination, the resonance peak is 2 dB higher than the initial value and the 3-dB bandwidth is increased to greater than 50 GHz. The low frequency rise in the response is caused by the limit of the on-chip capacitor. For data transmission with long word lengths, it is necessary to add a larger capacitor in parallel off chip to extend the low-frequency range. We have performed large signal modulation of digital data at 40 Gb/s non-return-to-zero (NRZ). The inset in Fig. 7 shows the observed modulated output for the device with 26  $\Omega$  operating in the forward traveling regime. The dynamic extinction ratio was 6 dB for a drive voltage of 1.6 V peak-to-peak

## 7. Conclusion

We have demonstrated a novel fabrication method for incorporating a p-InGaAs ohmic contact layer with an undercut-etched EAM. This device exhibits no reduction in efficiency due to the

narrowed waveguide after reducing the core width from 3 to 1.4  $\mu\text{m}$ . For a 600  $\mu\text{m}$  long device with matched termination, the 3-dB bandwidth was 34 GHz. To our knowledge, this is the longest InP-based EAM ever reported which is capable of modulation rates up to 40 Gb/s. The material structure and fabrication process used for this device allow for monolithic integration with SGDBR lasers for future generations of very high bandwidth widely tunable transmitters.